The Journal of Chemical Physics

Dynamics of an excitation-transfer trimer: Interference, coherence, Berry's phase development, and vibrational control of non-adiabaticity

Cite as: J. Chem. Phys. 158, 124307 (2023); https://doi.org/10.1063/5.0139174
Submitted: 18 December 2022 • Accepted: 28 February 2023 • Published Online: 24 March 2023

Jeffrey A. Cina

COLLECTIONS

Note: This paper is part of the JCP Special Topic on Celebrating 25 Years of Two-Dimensional Infrared (2D IR) Spectroscopy.

This paper was selected as an Editor's Pick

AIP Publishing

The Journal of Chemical Physics ARTICLE scitation.org/journal/jcp

Dynamics of an excitation-transfer trimer: Interference, coherence, Berry's phase development, and vibrational control of non-adiabaticity

Cite as: J. Chem. Phys. 158, 124307 (2023); doi: 10.1063/5.0139174
Submitted: 18 December 2022 • Accepted: 28 February 2023 •
Published Online: 24 March 2023

Jeffrey A. Cina[a)]

AFFILIATIONS

Department of Chemistry and Biochemistry, Oregon Center for Optical, Molecular, and Quantum Science, University of Oregon, Eugene, Oregon 97403, USA

Note: This paper is part of the JCP Special Topic on Celebrating 25 Years of Two-Dimensional Infrared (2D IR) Spectroscopy.
[a)]**Author to whom correspondence should be addressed:** cina@uoregon.edu

ABSTRACT

We detail several interesting features in the dynamics of an equilaterally shaped electronic excitation-transfer (EET) trimer with distance-dependent intermonomer excitation-transfer couplings. In the absence of electronic-vibrational coupling, symmetric and antisymmetric superpositions of two single-monomer excitations are shown to exhibit purely constructive, oscillatory, and purely destructive interference in the EET to the third monomer, respectively. In the former case, the transfer is modulated by motion in the symmetrical framework-expansion vibration induced by the Franck–Condon excitation. Distortions in the *shape* of the triangular framework degrade that coherent EET while activating excitation transfer in the latter case of an antisymmetric initial state. In its symmetrical configuration, two of the three single-exciton states of the trimer are degenerate. This degeneracy is broken by the Jahn–Teller-active framework distortions. The calculations illustrate closed, approximately circular pseudo-rotational wave-packet dynamics on both the lower and the upper adiabatic potential energy surfaces of the degenerate manifold, which lead to the acquisition after one cycle of physically meaningful geometric (Berry) phases of π. Another manifestation of Berry-phase development is seen in the evolution of the vibrational probability density of a wave packet on the lower Jahn–Teller adiabatic potential comprising a superposition of clockwise and counterclockwise circular motions. The circular pseudo-rotation on the upper cone is shown to stabilize the adiabatic electronic state against non-adiabatic internal conversion via the conical intersection, a dynamical process analogous to Slonczewski resonance. Strategies for initiating and monitoring these various dynamical processes experimentally using pre-resonant impulsive Raman excitation, short-pulse absorption, and multi-dimensional wave-packet interferometry are outlined in brief.

I. INTRODUCTION

From the earliest years of chemical physics, the paradigmatic process of electronic excitation transfer, involving, as it does, a complex interplay between electronic and nuclear dynamics, has been a perennial subject of experimental and theoretical investigation.[1,2] Many theoretical studies have focused on electronic energy transfer (EET) in molecular dimers embedded in condensed-phase media.[3–10] The transport of electronic excitation energy in a wide array of chromophoric multimers, including those responsible for natural solar-energy harvesting in photosynthesis, has been explored in computational simulations[11–14] and sophisticated ultrafast experiments,[15–17] with many of the latter representing revealing applications of multi-dimensional electronic spectroscopy.[18–22] Some of this work has led to worthwhile, extended conversations on the role of various types of coherence in electronic excitation transfer.[23,24]

While certain interesting features of energy-transfer in molecular trimers have been identified, symmetric (including equilateral) EET homo-trimers, in particular, do not appear to have been characterized as rigorously and comprehensively as dimers. Beyond its inherent interest as a molecular process in the smallest multimeric

host, excitation transfer in a cyclic trimer can be regarded as a model for EET dynamics in circular photosynthetic light-harvesting complexes.[15,16] This paper aims to provide a useful illustration of some of the unique dynamical processes that can occur in trimers and, by extension, in other small symmetrical EET systems. The experimental implementation of several of the dynamical processes considered here would rely on the ability to address, via laser-polarization selection, individual monomers within the complex having transition dipole moments that are not parallel with others. However, it is possible that similar processes could be observed in small arrays of trapped atomic ions,[25–28] utilizing direct excitation with tightly focused laser beams.

The main text of this paper begins by introducing the Hamiltonian operator for an equilateral triangular trimer with intermonomer distance-dependent electronic excitation-transfer couplings. Normal coordinates are identified, which comprise symmetric expansion and contraction of the trimer, along with shape-changing coordinates responsible for scalene and isosceles distortions. The electronic Hamiltonian is broken down into portions that exclude and include the effects of changes in the EET coupling due to the distortion coordinates. The former portion is diagonalized to obtain singly excited exciton states that prove useful for further description. Two of these single-exciton states are found to be degenerate and subject to Jahn–Teller splitting through the latter portion of the Hamiltonian when framework distortions break the equilateral symmetry. To facilitate selective excitation and probing, the monomers are ascribed to have mutually perpendicular electronic transition dipole moments.

Section III explores the effects of multi-path interference in the electronic excitation transfer from the initial singly excited states comprising coherent superpositions of different site-excited states. In the absence of asymmetric framework-distortion dynamics, the sum and difference superpositions of two site-states are shown to exhibit an oscillatory excitation transfer to the third monomer, due to constructive interference, and no excitation transfer to the third monomer, due to destructive interference, respectively. Framework-distortion dynamics is then shown to diminish the excitation transfer from the sum state and to *enable* excitation transfer from the difference state.

With an eye toward molecular geometric-phase development, nearly adiabatic dynamics on the trimer's lower Jahn–Teller surface is considered in the section after that. A practical explanation is provided of how the adiabatic electronic eigenstates of spatially varying composition can be made to change continuously and rendered single-valued with respect to the nuclear coordinates. Further exposition is given of how, using polarization selection, a nuclear wave packet can be launched on a chosen excited adiabatic potential from a moving ground-state packet. Cyclic distortion-mode pseudo-rotation about the conical intersection, a desired state of motion for the direct experimental observation of geometric/Berry-phase acquisition,[29–35] is illustrated. A less direct physical manifestation of geometric-phase accumulation is demonstrated in the destructive interference between superposed clockwise- and counterclockwise-moving packets upon their completion of half-odd numbers of pseudo-rotational cycles.

The possible exertion of dynamical control over the non-adiabatic transitions from the trimer's upper to its lower Jahn–Teller surface is the last topic considered. Based on an analogy with the stabilization against the non-adiabatic decay of the upper-surface Born–Oppenheimer-like molecular eigenstates of large pseudo-rotational angular momentum, which are known to exhibit Slonczewski resonances,[36] we investigate the time-evolution of pseudo-rotating upper-surface wave packets whose motion circles the intersection point. Time-dependent states of this kind are contrasted with upper-surface wave packets of similar vibrational energy that undergo *linear* motion and, at first, move away from the conical intersection, at the cost of passing through it afterward.

In a concluding discussion, we entertain the prospects for experimental tests of the various predicted dynamical processes using multi-dimensional wave-packet interferometry and other ultrafast spectroscopic methods. The necessary future elaborations of the illustrative trimer model are also briefly outlined, and the connections with the work of others are discussed.

II. MODEL TRIMER

We employ a simple model of an equilaterally shaped excitation-transfer trimer in order investigate the effects of dynamical changes in the size and shape of a symmetrical complex upon multi-path interference in energy transfer, geometric-phase acquisition, and non-adiabatic decay during coherent pseudo-rotation within a Jahn–Teller-active degenerate manifold of singly electronically excited states. The trimer, shown schematically in Fig. 1, comprises identical molecular chromophores a, b, and c, each with ground and excited electronic levels g and e. We denote the eight electronic site-states of the trimer as $|G\rangle = |ggg\rangle$, $|A\rangle = |egg\rangle$, $|B\rangle = |geg\rangle$, $|C\rangle = |gge\rangle$, $|\bar{A}\rangle = |gee\rangle$, $|\bar{B}\rangle = |ege\rangle$, $|\bar{C}\rangle = |eeg\rangle$, and $|E\rangle = |eee\rangle$. The monomers are confined to a plane and separated by a mass-weighted distance L at their equilibrium positions in the G-state. They are bound together by pairwise harmonic potentials of frequency Ω, with $\sqrt{\hbar/2\Omega} \ll L$. We assume that the coupling strength for energy transfer between excited and unexcited monomers, $J(R_{ij}) = J_0 + J_1(R_{ij} - L)$, depends linearly on distance in the same way, whether or not the third monomer is electronically excited.

Starting with a system of two-dimensional Cartesian coordinates for the location of each monomer, carrying out a normal-mode

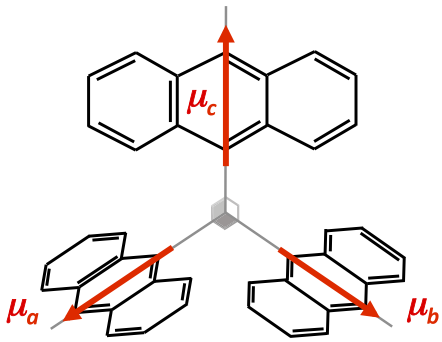

FIG. 1. Energy-transfer trimer whose monomers are arranged in an equilateral triangular configuration with nonparallel (here, mutually perpendicular) transition dipole moments.

analysis, and discarding the overall translational and rotational modes lead to the trimer Hamiltonian

$$H = \frac{p^T p}{2} + H_{el}(q). \tag{1}$$

The components of the vectors,

$$p = \begin{pmatrix} p_{sym} \\ p_{scal} \\ p_{isos} \end{pmatrix} \quad \text{and} \quad q = \begin{pmatrix} q_{sym} \\ q_{scal} \\ q_{isos} \end{pmatrix}, \tag{2}$$

are the normal momenta and coordinates for symmetric expansion, and the scalene and isosceles distortions of the three-monomer framework are shown in Fig. 2. These correspond to the familiar vibrational modes of an equilateral triatomic molecule.

The electronic Hamiltonian is given by

$$H_{el}(q) = H_0(q) + H_1(q). \tag{3}$$

In the first term of Eq. (3), mixing among the singly and doubly excited site-states is symmetrical,

$$\begin{aligned} H_0(q) = {} & \frac{\omega_{sym}^2}{2} q_{sym}^2 + \frac{\omega^2}{2}\left(q_{scal}^2 + q_{isos}^2\right) \\ & + \upsilon\left(|A\rangle\langle A| + |B\rangle\langle B| + |C\rangle\langle C|\right) \\ & + \bar{\upsilon}\left(|\bar{A}\rangle\langle\bar{A}| + |\bar{B}\rangle\langle\bar{B}| + |\bar{C}\rangle\langle\bar{C}|\right) + \bar{\bar{\upsilon}}\,|E\rangle\langle E| \\ & + (J_0 + J_1 q_{sym})\big[\left(|B\rangle\langle A| + |C\rangle\langle B| + |A\rangle\langle C|\right. \\ & \left. + |\bar{A}\rangle\langle\bar{B}| + |\bar{B}\rangle\langle\bar{C}| + |\bar{C}\rangle\langle\bar{A}|\right) + \text{H.c.}\big], \end{aligned} \tag{4}$$

where $\omega_{sym} = \sqrt{3}\,\Omega$ and $\omega = \sqrt{\frac{3}{2}}\,\Omega$ are the symmetric- and distortion-mode frequencies, respectively, and the upsilons are bare electronic energies. The second term in Eq. (3) accounts for the effects upon excitation transfer of differing changes in the inter-monomer distance within the a–b, b–c, and c–a pairs due to scalene and isosceles distortions,

$$\begin{aligned} H_1(q) = {} & -J_1 q_{isos}\left[\left(|B\rangle\langle A| + |\bar{A}\rangle\langle\bar{B}|\right) + \text{H.c.}\right] \\ & + J_1\left(-\frac{\sqrt{3}}{2} q_{scal} + \frac{1}{2} q_{isos}\right)\left[\left(|C\rangle\langle B| + |\bar{B}\rangle\langle\bar{C}|\right) + \text{H.c.}\right] \\ & + J_1\left(\frac{\sqrt{3}}{2} q_{scal} + \frac{1}{2} q_{isos}\right)\left[\left(|A\rangle\langle C| + |\bar{C}\rangle\langle\bar{A}|\right) + \text{H.c.}\right]. \end{aligned} \tag{5}$$

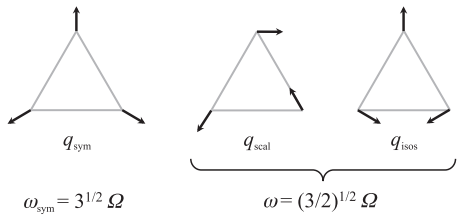

FIG. 2. Normal coordinates of the excitation-transfer trimer, including the nondegenerate symmetric vibration and the degenerate framework-distortion modes.

While $H_1(q)$ will not be treated through a perturbation-theory expansion, it is, nonetheless, useful to determine the eigenstates of $H_0(q)$. In this paper, the focus will be on the unexcited and singly excited electronic states. The electronic ground state $|G\rangle$ remains an eigenket of $H_0(q)$, with energy $\epsilon_G(q) = \frac{\omega_{sym}^2}{2} q_{sym}^2 + \frac{\omega^2}{2}\rho^2$. The singly excited eigenkets of $H_0(q)$ are the excitonic states

$$|+\rangle = \frac{1}{\sqrt{3}}\left(|A\rangle\, e^{i\frac{5\pi}{12}} + |B\rangle\, e^{-i\frac{11\pi}{12}} + |C\rangle\, e^{-i\frac{\pi}{4}}\right), \tag{6}$$

$$|-\rangle = \frac{1}{\sqrt{3}}\left(|A\rangle\, e^{-i\frac{5\pi}{12}} + |B\rangle\, e^{i\frac{11\pi}{12}} + |C\rangle\, e^{i\frac{\pi}{4}}\right), \tag{7}$$

and

$$|0\rangle = \frac{1}{\sqrt{3}}\left(|A\rangle + |B\rangle + |C\rangle\right), \tag{8}$$

with energies

$$\epsilon_+(q) = \epsilon_-(q) = \upsilon + \frac{\omega_{sym}^2}{2} q_{sym}^2 + \frac{\omega^2}{2}\rho^2 - (J_0 + J_1 q_{sym}) \tag{9}$$

and

$$\epsilon_0(q) = \upsilon + \frac{\omega_{sym}^2}{2} q_{sym}^2 + \frac{\omega^2}{2}\rho^2 + 2(J_0 + J_1 q_{sym}). \tag{10}$$

We have introduced cylindrical distortion-mode coordinates with $q_{scal} = \rho\cos\varphi$ and $q_{isos} = \rho\sin\varphi$. It is interesting to observe that the eigenkets of $H_0(q)$ given in Eqs. (6)–(8) remain independent of the nuclear coordinates q.

Within the space spanned by the ground and singly excited states, the zeroth-order electronic Hamiltonian can now be written as

$$H_0(q) = |G\rangle\epsilon_G(q)\langle G| + \sum_{\sigma=0,\pm} |\sigma\rangle\epsilon_\sigma(q)\langle\sigma|. \tag{11}$$

Writing the first-order electronic Hamiltonian in the exciton basis,

$$\begin{aligned} H_1(q) = {} & J_1\rho\left(|+\rangle\langle -|e^{-i\varphi} + |-\rangle\langle +|e^{i\varphi}\right) \\ & + \frac{J_1\rho}{2}\left[\left(|0\rangle\langle +| + |-\rangle\langle 0|\right)e^{-i\varphi + i\frac{\pi}{4}} + H.c.\right], \end{aligned} \tag{12}$$

reveals that the triangular symmetry-breaking distortions effect a Jahn–Teller coupling within the degenerate plus/minus exciton manifold and also couple the degenerate and nondegenerate excitonic states. The former effects will be larger than the latter, as the splitting between the degenerate and nondegenerate excitonic manifolds goes as $\sim 3(J_0 + J_1 q_{sym})$, which is assumed to be larger than $J_1\rho$.

In the electronic subspace spanned by the ground and singly excited states, the dipole moment operator is given by

$$\begin{aligned} \hat{\mu} = {} & \hat{\boldsymbol{\mu}}_a + \hat{\boldsymbol{\mu}}_b + \hat{\boldsymbol{\mu}}_c \\ = {} & \mu\mathbf{e}_a\left(|A\rangle\langle G| + |G\rangle\langle A|\right) + \mu\mathbf{e}_b\left(|B\rangle\langle G| + |G\rangle\langle B|\right) \\ & + \mu\mathbf{e}_c\left(|C\rangle\langle G| + |G\rangle\langle C|\right). \end{aligned} \tag{13}$$

For present purposes, the unit vectors $\mathbf{e}_a$, $\mathbf{e}_b$, and $\mathbf{e}_c$ are taken to be mutually perpendicular, but any symmetrical arrangement in which they span three-dimensional space would suffice.

III. WHICH-PATH INTERFERENCE IN EXCITATION TRANSFER

The model trimer provides a test-bed for studying multi-path interference in electronic excitation transfer. From the sum and difference superposition states $\frac{1}{\sqrt{2}}(|A\rangle + |B\rangle)$ and $\frac{1}{\sqrt{2}}(|A\rangle - |B\rangle)$, for instance, one might anticipate constructive and destructive "two-slit" interference, respectively, in energy transfer to monomer c. Those initial states could be prepared by short-pulse absorption with the respective laser polarizations $\frac{1}{\sqrt{2}}(\mathbf{e}_a + \mathbf{e}_b)$ and $\frac{1}{\sqrt{2}}(\mathbf{e}_a - \mathbf{e}_b)$. The situation will be complicated by the simultaneous occurrence of $a \rightarrow b$ and $a \leftarrow b$ excitation transfer, however. Interesting effects are also to be expected from the Franck–Condon activation of the symmetric and distortional framework vibrations following the short-pulse electronic excitation, which, through the distance-dependence of the EET couplings, influence the intermonomer electronic energy transfer.

Figure 3 plots the time-evolution of the C-state population under $\frac{1}{2}p^T p + H_0(q)$ (gray) and $\frac{1}{2}p^T p + H_0(q) + H_1(q)$ (black), starting from the normalized sum of site-states A and B times the nuclear ground state $|0_{sym}\rangle|0_{scal}\rangle|0_{isos}\rangle$. These and the other calculations in this section were carried out by diagonalizing the trimer Hamiltonian in a basis of excitonic states and 1D eigenstates for the symmetric, scalene, and isosceles vibrations represented on uniformly spaced discrete position grids. The zeroth-order EET coupling constant was assigned the value $J_0 = 8\hbar\Omega$. The parameter determining energy transfer's distance dependence was set to $J_1 = -\sqrt{2\hbar\Omega^3}$.

Both calculations exhibit episodes of coherent out-and-back population of the C-state at frequency $\sim 3J_0/\hbar$, corresponding to the approximate splitting between degenerate and nondegenerate exciton states. Even in the absence of the distortion-mode dynamics governed by $H_1(q)$, coherent population transfer is turned off and on at frequency ω_{sym} as a result of the periodic loss and regaining of the overlap between the symmetric-mode wave functions

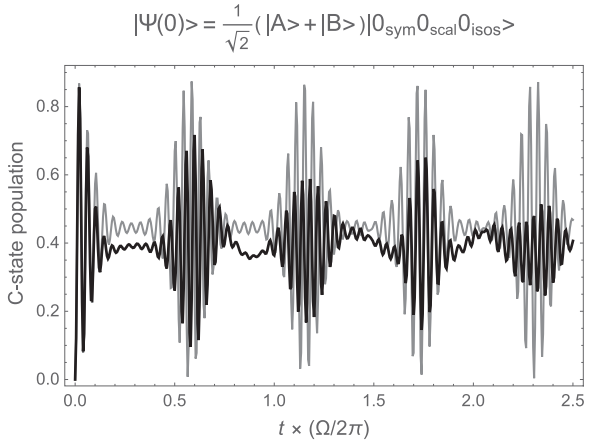

FIG. 3. Population of the C-state as a function of time, starting from a symmetric superposition of the A and B electronic states. Dynamics excluding (including) dependence of the EET coupling elements on the framework-distortion modes is shown in gray (black).

accompanying the degenerate and nondegenerate excitonic components, due to their differing Franck–Condon displacements (J_1/ω_{sym}^2 and $-2J_1/\omega_{sym}^2$, respectively) in the symmetric framework-expansion vibration [see Eqs. (9) and (10)]. The maximum C-state population is seen to be about 0.89, rather than unity.

These features can be understood by using Eqs. (6)–(8) to write

$$\frac{|A\rangle + |B\rangle}{\sqrt{2}} = -\frac{1}{\sqrt{3}}|\xi\rangle + \sqrt{\frac{2}{3}}|0\rangle, \tag{14}$$

$$\frac{|A\rangle - |B\rangle}{\sqrt{2}} = |\tilde{\xi}\rangle, \tag{15}$$

and

$$|C\rangle = \sqrt{\frac{2}{3}}|\xi\rangle + \frac{1}{\sqrt{3}}|0\rangle. \tag{16}$$

Here,

$$|\xi\rangle = \frac{1}{\sqrt{2}}\left(|+\rangle e^{i\frac{\pi}{4}} + |-\rangle e^{-i\frac{\pi}{4}}\right) \tag{17}$$

and

$$|\tilde{\xi}\rangle = \frac{1}{\sqrt{2}}\left(|+\rangle e^{-i\frac{\pi}{4}} + |-\rangle e^{i\frac{\pi}{4}}\right) \tag{18}$$

are alternative eigenkets of $H_0(q)$ with energies $\epsilon_\xi(q) = \epsilon_{\tilde{\xi}}(q) = \epsilon_\pm(q)$ [see Eq. (9)]. The probability amplitude in C starting from the sum-state becomes

$$\begin{aligned}\langle C|\Psi_{sum}(t)\rangle &= \left\langle C|e^{-\frac{it}{\hbar}\left[\frac{1}{2}p^T p + H_0(q) + H_1(q)\right]}\frac{1}{\sqrt{2}}(|A\rangle + |B\rangle)|0_{sym}0_{scal}0_{isos}\right\rangle \\ &\cong \frac{\sqrt{2}}{3}\left\{e^{-\frac{it}{\hbar}\left[\frac{1}{2}p^T p + \epsilon_0(q)\right]} - \left\langle\xi|e^{-\frac{it}{\hbar}\left[\frac{1}{2}p^T p + \epsilon_\xi(q) + H_1(q)\right]}|\xi\right\rangle\right\} \\ &\quad \times |0_{sym}0_{scal}0_{isos}\rangle\Big\rangle,\end{aligned} \tag{19}$$

where, in the second equality, we have neglected the small effects by which H_1 couples the degenerate and nondegenerate excitonic manifolds. Neglecting H_1 altogether, as in the gray curve of Fig. 3, gives an approximate C-state population,

$$\begin{aligned}&\langle\Psi_{sum}^{(0)}(t)|C\rangle\langle C|\Psi_{sum}^{(0)}(t)\rangle \\ &= \frac{4}{9}\left\{1 - \mathrm{Re}\left[e^{\frac{it}{\hbar}3J_0}\langle 0_{sym}|e^{\frac{it}{\hbar}\left(\frac{1}{2}p_{sym}^2 + \frac{1}{2}\omega_{sym}^2 q_{sym}^2 + 2J_1 q_{sym}\right)}\right.\right. \\ &\quad \left.\left. \times e^{-\frac{it}{\hbar}\left(\frac{1}{2}p_{sym}^2 + \frac{1}{2}\omega_{sym}^2 q_{sym}^2 - J_1 q_{sym}\right)}|0_{sym}\rangle\right]\right\},\end{aligned} \tag{20}$$

which can be evaluated analytically. A key point is that the C-state population becomes $8/9 = 0.888$, rather than unity, when the wave-packet overlap in square brackets takes the value -1. The diminution over time of the bursts of oscillatory excitation transfer, seen in the black curve of Fig. 3, results from the degradation of the second term in braces in Eq. (19) by Jahn–Teller dynamics in the framework-distortion modes.

Since the electronic portion of the difference superposition state,

$$|\Psi_{diff}(0)\rangle = \frac{|A\rangle - |B\rangle}{\sqrt{2}}|0_{sym}0_{scal}0_{isos}\rangle = |\bar{\xi}\rangle|0_{sym}0_{scal}0_{isos}\rangle, \qquad (21)$$

is orthogonal to both $|\xi\rangle$ and $|0\rangle$, the excitation transfer to site c cannot occur in the absence of coupling to the framework distortions, as shown by the dashed line in Fig. 4. Nuclear motion at the symmetric- and distortion-mode periods of $\Omega/\omega_{sym} \cong 0.577$ and $\Omega/\omega \cong 0.816$, respectively, is evident in the solid curve of Fig. 4, which includes distortional effects on the EET coupling, along with a delayed onset of a small amount of coherent excitation exchange at the frequency $\sim 3J_0/\hbar$.

It will perhaps be worthwhile in future studies to consider whether the electronic coherence in a multi-chromophoric array,[37,38] imposed externally by exciting-laser polarization, could be used to influence the *directionality* of the excitation transfer to a targeted acceptor by a near-field mechanism akin to wave-vector matching. In an interesting recent report, Tomasi and Kassal[39] investigated the effects of the initial intersite vs interexciton coherence upon the relative efficiency of recombination and excitation-trapping in multi-chromophore systems characterized by site-based or exciton-based dissipation. Cao and Silbey[40] examined cases of varied signs of coupling elements within a trimeric excitation donor as an illustration of their general theory of excitation transfer and trapping kinetics. As an application of his polaronic quantum master equation theory, Jang treated a case of donor–bridge–acceptor excitation transmission.[41] A recent report by Engelhardt and Cao[42] explores the effects of both dephasing and the Aharonov–Bohm effect on the steady-state current- and waiting-time distribution of electron transport through a three-site mesoscopic system. In another study, Hossein Nejad *et al.*[43] evaluated the effects of the interference between the direct and indirect pathways on the excitation transfer between donor and acceptor chromophores.

Thorough studies of multi-path interference in molecular *electron* transfer have led to the conclusion that Coulombic interactions with moving charges tend to leave a strong enough imprint on the surrounding medium to record its path and thereby extinguish the quantum mechanical interference effects in the transfer probability.[44,45]

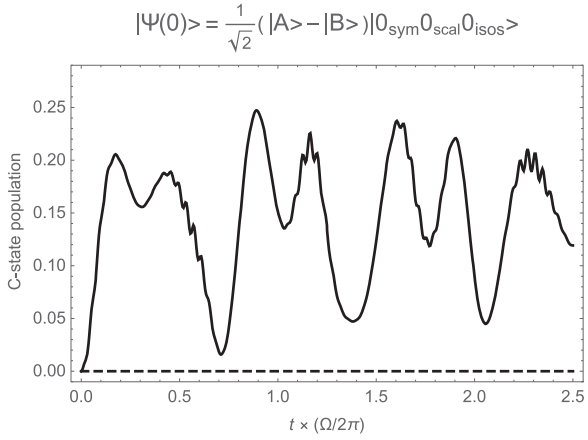

FIG. 4. Population of C starting from a difference-state superposition of A and B. Dynamics excluding (including) the dependence of the EET coupling on the framework-distortion modes is plotted with a dashed (solid) line.

IV. NEARLY ADIABATIC DYNAMICS ON THE LOWER JAHN–TELLER SURFACE

Section III considered the evolving populations in different excitonic or site states, fixed singly excited electronic states whose identities do not change with the size and shape of the trimer. In this section and the next one, we examine the motion of nuclear wave packets associated with different adiabatic electronic states, excited states whose compositions are slaved to the nuclear configuration.

Adiabatic electronic eigenenergies and eigenkets are found by diagonalizing the electronic Hamiltonian of Eq. (3) for various nuclear arrangements $q = (q_{sym}, q_{scal}, q_{isos})$. Figure 5 shows the singly excited eigenenergies $E_+(q)$, $E_-(q)$, and $E_0(q)$ as functions of (q_{scal}, q_{isos}) for the value $q_{sym} = J_1/\omega_{sym}^2$; although it may not be obvious from the figure, these potential energy surfaces are not strictly cylindrically symmetric, due to the terms in $H_1(q)$ that couple degenerate and nondegenerate excitonic states. While the E_0 surface resembles the harmonic distortion potential $\frac{1}{2}\omega^2(q_{scal}^2 + q_{isos}^2)$ of the electronic ground state (absent in its slight departure from cylindrical symmetry), E_+ and E_- participate in a conical intersection at the equilateral configuration $(q_{scal}, q_{isos}) = (0, 0)$.

While the electronic eigenenergies $E_\sigma(q)$ and $E_\sigma(q + \delta q)$ for nearby nuclear configurations have similar values, the corresponding adiabatic electronic *states* for adjacent configurations that are returned by numerically diagonalizing $H_{el}(q)$ may be given unrelated overall phase factors. In order to describe nuclear wave packets

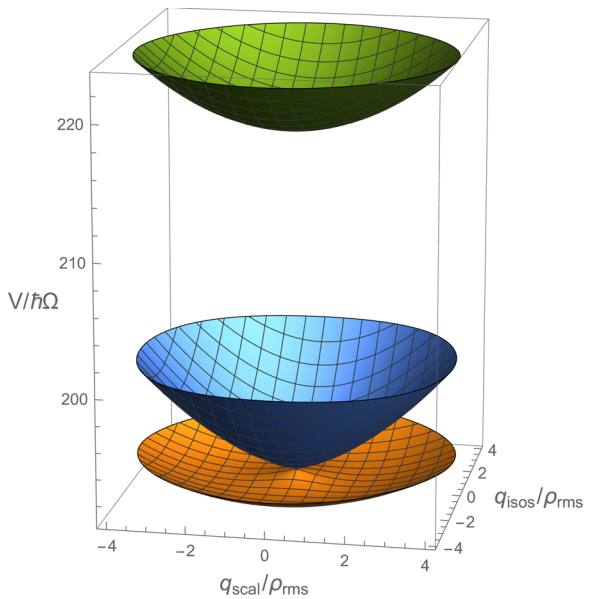

FIG. 5. Adiabatic electronic potential energy surfaces $E_+(J_1/\omega_{sym}^2, q_{scal}, q_{isos})$ (orange), $E_-(J_1/\omega_{sym}^2, q_{scal}, q_{isos})$ (blue), and $E_0(J_1/\omega_{sym}^2, q_{scal}, q_{isos})$ (green) for the energy-transfer trimer. The bare electronic energy is assigned the value $\upsilon = 200\ \hbar\Omega$ and $\rho_{rms} \equiv \sqrt{\hbar/2\omega}$.

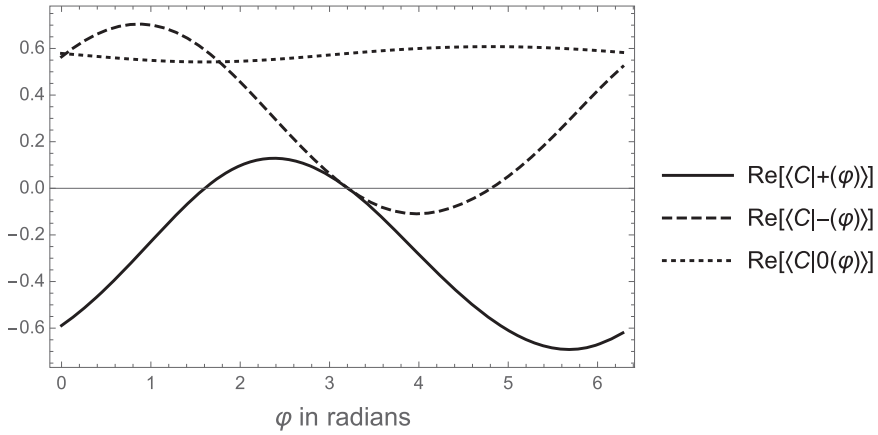

FIG. 6. Real part of the amplitude of each of the singly excited adiabatic electronic eigenstates in the site-state C. The curves manifest the continuity and single-valuedness of $|+(q)\rangle$, $|-(q)\rangle$, and $|0(q)\rangle$ along closed paths from $\varphi = 0$ to 2π (with $q_{sym} = J_1/\omega_{sym}^2$ and $\rho = -J_1/\omega^2$), which, in the first two instances, encircle a conical intersection.

associated with different adiabatic potential energy surfaces, a rule must be imposed on the coordinate-dependent phase of each $|\sigma(q)\rangle$ that renders the electronic state single-valued and amenable to numerical differentiation as a function of q.

To address this issue, we first solved the three-by-three electronic Schrödinger equation on a grid of nuclear configurations $q = (q_{sym}, \rho, \varphi)$ and then shifted the phases of the σth adiabatic electronic states for different nuclear configurations, starting from the one at an arbitrary reference point q_0, so that each state has a positive, real-valued overlap (near unity) with adiabatic states of the same electronic index for adjacent q values. As expected based on the general analyses of adiabatic phase factors, it was found that this procedure led to violations of single-valuedness: for $\sigma = +$ or $-$, the last adiabatic state in a closed, single-loop path around the point of conical intersection differed in sign from the otherwise nearly identical first state, a problem that was not encountered with the nondegenerating $|0(q)\rangle$.

This shortcoming was easily corrected on our spatial grid, which utilizes cylindrical distortion-mode coordinates. The coordinate-dependent states for $\sigma = +$ or $-$ were multiplied by phase factors $e^{i(n_\sigma + \frac{1}{2})\varphi}$ featuring an arbitrary half-odd multiple of the azimuthal angle. As illustrated in Fig. 6, this strategy leads to excited adiabatic electronic states that vary continuously with nuclear configuration while maintaining single-valuedness.

Treating the dynamics of our model trimer with adiabatic electronic states and their accompanying nuclear wave packets does not confer a significant computational advantage, as it could for a larger system. It is physically illuminating, nonetheless, to describe the initial-state preparation and subsequent evolution in those terms, while *calculating* the time-dependent state by decomposing it in a basis of vibronic eigenstates.

To this end, we find the eigenstates and energies of the full trimer Hamiltonian of Eq. (1), within the singly electronically excited manifold, in a basis of excitonic states and one-dimensional symmetric-mode and radial and angular distortion-mode nuclear eigenstates appropriate to the electronic ground state, with each of the nuclear factors being sampled on the same grid over which adiabatic electronic states are evaluated above. It is, then, straightforward to express a chosen initial state of the trimer as a superposition of eigenfunction components and take an inner product with a particular adiabatic electronic eigenstate at any later time to find the associated time-propagated nuclear wave packet.

A. Cyclic shape-changes: Coherent pseudo-rotation

The change in the sign of the electronic wave function upon adiabatic encirclement of a conical intersection,[29,30] which can be equivalently described as the development of a Berry phase equal to π,[32,35] has long been a subject of interest in molecular physics. Cina, Smith, and Romero-Rochín put forward a strategy for directly tracking the time-development of this nontrivial geometric phase.[46–48] Their approach, which has not yet been implemented, relies on the short-pulse electronic excitation of a pseudo-rotating nuclear wave packet with pairs of phase-locked laser pulses of variable intrapulse-pair delay. A copy of this wave packet generated by one sub-pulse—the target—encircles a conical intersection between the excited-state adiabatic surfaces and interferes with a reference packet prepared by the other sub-pulse. Those authors showed that the resulting fluorescence-detected wave-packet interferometry signal could monitor excited-state dynamics at the level of amplitudes, including geometric-phase acquisition, rather than probability densities.

The classical equations of motion on the adiabatic distortion-mode potentials, temporarily stripped of their slight cylindrical asymmetries, show that closed circular trajectories of radius ρ_{circ} occur with angular velocities

$$\dot{\varphi}_+ = \pm\sqrt{\frac{\omega^2\rho_{circ} + J_1}{\rho_{circ}}} \quad \left(\text{for } \rho_{circ} > -\frac{J_1}{\omega^2}\right), \tag{22}$$

$$\dot{\varphi}_- = \pm\sqrt{\frac{\omega^2\rho_{circ} - J_1}{\rho_{circ}}} \quad \left(\text{for } \rho_{circ} > \frac{J_1}{\omega^2}\right), \tag{23}$$

and

$$\dot{\varphi}_0 = \pm\omega\rho_{circ}, \tag{24}$$

on the plus-, minus-, and zero-surfaces, respectively. Based on these classical trajectories, we can define the initial conditions for approximately circular distortion-mode wave-packet dynamics—molecular pseudo-rotation—on any of the three singly excited surfaces. In this

section, we investigate the distortional pseudo-rotation of the trimer on $E_+(q)$ (with the same Hamiltonian parameters as before), setting the stage for future studies of electronic geometric phase acquisition and its measurement by optically phase-coherent ultrafast spectroscopy. Although the ultimate origin of molecular Berry-phases resides within the Born–Oppenheimer approximation,[49] it is hoped that the prospects raised here will motivate tests demonstrating that geometric-phase accumulation by nuclear wave packets in the presence of conically intersecting potential energy surfaces remains a physically meaningful manifestation of adiabatic dynamics. Pseudo-rotation on the upper cone $E_-(q)$, which should also give rise to geometric phase development, is explored in Sec. V, in order to study the effects of the initial conditions of nuclear motion on non-adiabatic decay to $E_+(q)$.

A nuclear wave packet with positions and momenta localized around chosen values could be launched on a selected excited-state adiabatic potential by short-pulse electronic absorption from an appropriately moving packet in the G-state (prepared, for instance, by sequential pre-resonant impulsive Raman excitation). Because the matrix elements of the dipole moment operator components between $|G\rangle$ and each of the $|\sigma(q)\rangle$ are nuclear-coordinate dependent, laser polarization (along with spectral content) plays an important role in adiabatic target-state selection. Polarization selection will be based on the central location q_0 of the ground-state wave packet at the time of short-pulse electronic excitation. However, since the packet has nonzero width, its edges may undergo amplitude-transfer to other than the nominally selected surface (the resulting imperfect adiabatic-state selection could be mitigated by the finite spectral bandwidth of the exciting pulse).

In order to investigate nearly circular pseudo-rotation in the lowest adiabatic electronic excited state, we imagine starting with a nuclear wave packet $|\psi_G(0)\rangle$ in G, displaced by J_1/ω_{sym}^2 in q_{sym}, with the time-zero expectation value of q_{scal} equal to $\rho_{circ} = -2J_1/\omega^2$, and that of p_{isos} set to $\rho_{circ}\,\dot{\varphi}_+ = \sqrt{\rho_{circ}(\omega^2\rho_{circ} + J_1)}$. This packet would be executing *elliptical* pseudo-rotation in the electronic ground-state,

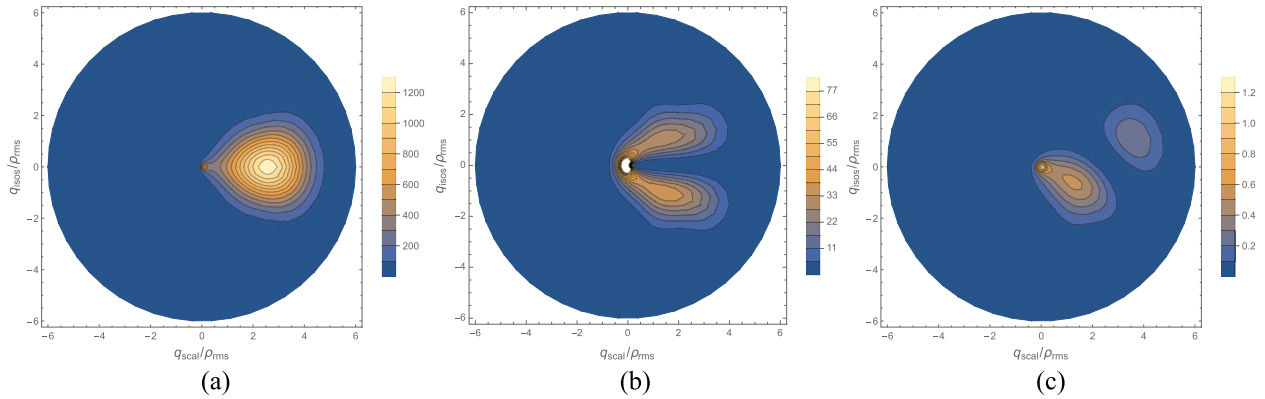

FIG. 7. Distortion-mode nuclear probability density on the plus (a), minus (b), and zero (c) singly excited adiabatic potential energy surfaces, prepared by short-pulse excitation from the electronic ground state of a wave packet displaced in the scalene mode with isosceles-mode momentum chosen to give rise to nearly circular pseudo-rotation in the plus-state. Note the much smaller probability densities in the (deselected) minus- and zero-states.

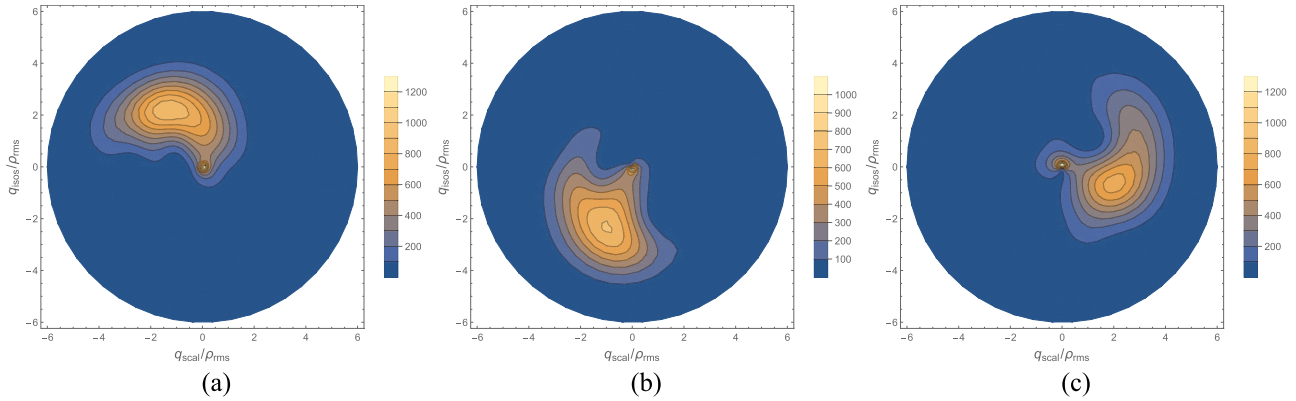

FIG. 8. Distortion-mode nuclear probability densities on the plus-state adiabatic surface at one-third (a), two-thirds (b), and three-thirds (c) of the classical period for circular pseudo-rotation at the chosen displacement.

while undergoing coherent oscillatory motion in the symmetric mode. The time-zero displacement of the symmetric mode is chosen to match the common minimum position of the degenerate excitonic states so that, upon electronic excitation, little oscillatory expansion and contraction of the trimer ensue within the degenerate manifold. The desired polarization direction is determined from $\boldsymbol{\mu}_0 \equiv \langle +(J_1/\omega_{sym}^2, \rho_{circ}, 0)|\hat{\mu}|G\rangle$, and the starting nuclear wave packets in the three excitonic states are evaluated from $\frac{\hat{\mu}\cdot\boldsymbol{\mu}_0}{\mu^2}|G\rangle|\psi_G(0)\rangle$, without using pulse propagators[50,22] to account for the effects of finite spectral bandwidth.

In our examination of the ensuing distortion-mode dynamics in the adiabatic electronic excited states, we take advantage of the immobility of the symmetric mode in the plus- and minus-adiabatic states and evaluate the appropriate three-dimensional nuclear wave functions at $q_{sym} = J_1/\omega_{sym}^2$, rather than calculating an inner product with a symmetric-mode wave function. Figure 7 plots the resulting time-zero 2D nuclear probability densities in all three adiabatic electronic excited states. It is seen that, with the chosen excitation polarization, most of the excited-state probability density resides on the lowest (plus) Jahn–Teller surface. A small amount of density

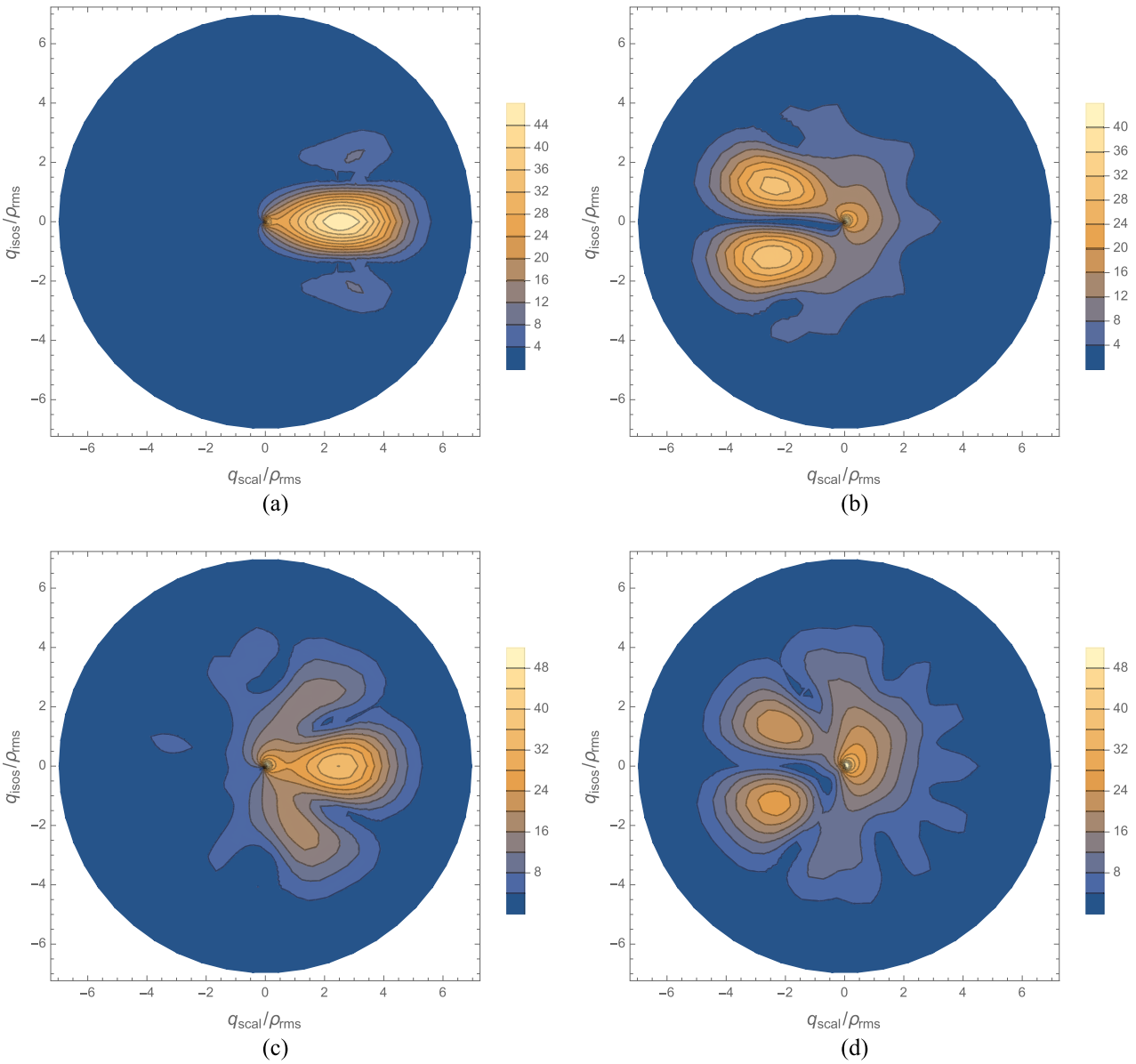

FIG. 9. Left to right in upper and lower rows are the contour plots of the absolute value of an evolving double wave packet on the plus adiabatic surface at intervals of one-half the period for circular pseudo-rotation. The initial distortion-modes packet superposes equal amplitudes moving in clockwise and counterclockwise directions. Destructive interference at half-odd-period propagation times is an observable consequence of geometric-phase acquisition under adiabatic dynamics.

is generated on the upper cone (minus-potential), and a negligible probability density is created in the zero-state. Largely adiabatic dynamics on the lowest surface follows, as shown in Fig. 8, and it consists of nearly circular pseudo-rotation, as the classical prediction suggests.

Cyclic pseudo-rotation about a conical intersection would be useful in seeking to observe an adiabatic geometric-phase accumulation by the corresponding complex-valued nuclear amplitude with the optical phase-controlled ultrafast spectroscopy.[46–48] An experimental test of this kind would involve monitoring the contribution to the excited-state population due to the interference between a pseudo-rotating wave packet that acquires a geometric phase and another one that does not. While the original exploration of this strategy[46] promoted circularly pseudo-rotating wave packets in the electronic ground-state to a Jahn–Teller-active excited state and relied on the trough of that potential to channel wave-packet motion, the predictions of this section show that more advantageous, nearly circular trajectories of any radius around the conical intersection are also possible. This amplitude-level physical consequence of adiabatic nuclear dynamics on a potential surface participating in a conical intersection would also be manifested in a complete experimental reconstruction of the evolving nuclear wave packet on that surface.[51,52]

B. Geometric/Berry-phase interference effects in double wave packets

It is possible to envisage the observation of the less direct consequences of geometric-phase development in this energy-transfer trimer. In this subsection, we examine the time-evolution of a superposition of *two* circularly pseudo-rotating distortion-mode wave packets on the trimer's lower Jahn–Teller surface. Figure 9 explores the propagation of a wave packet in the plus-adiabatic state that was launched by a short-pulse excitation from a wave packet in G comprising a superposition of packets having equal amplitudes with the expectation value of p_{isos} set to $+\sqrt{\rho_{circ}(\omega^2\rho_{circ}+J_1)}$ and $-\sqrt{\rho_{circ}(\omega^2\rho_{circ}+J_1)}$, which are otherwise identical to the one considered in Sec. IV A. This figure plots the absolute value of the nuclear probability amplitude rather than the probability density.

As a result of their acquisition of equal and opposite geometric phase factors (i.e., phase factors differing in sign, such as $e^{i\frac{\pi}{2}} = i$ and $e^{-i\frac{\pi}{2}} = -i$), the clockwise- and counterclockwise-moving wave packets are seen to interfere destructively in the vicinity of $\varphi = \pi$ after half-odd multiples of the pseudo-rotation period $\tau_+ = 2\pi/\dot{\varphi}_+ = 2\pi\sqrt{\rho_{circ}/(\omega^2\rho_{circ}+J_1)}$. Hence, the geometric-phase acquisition leads, in this instance, to *zero probability* for the trimer to have a negative value of the scalene distortion coordinate in the absence of an accompanying isosceles deformation. This observable consequence of the nuclear dynamics in the presence of a conical intersection is in keeping with the prior predictions by Izmaylov and co-workers on the effects of geometric-phase development in chemical reaction dynamics[53,54] and transport phenomena.[55]

In order to emphasize the fact that the destructive interference predicted in Fig. 9 is a physical manifestation of Berry-phase acquisition rather than an artifact of an adiabatic *description*, we contrast it with the corresponding wave-packet evolution on a similarly shaped potential surface that *does not* participate in a conical intersection.

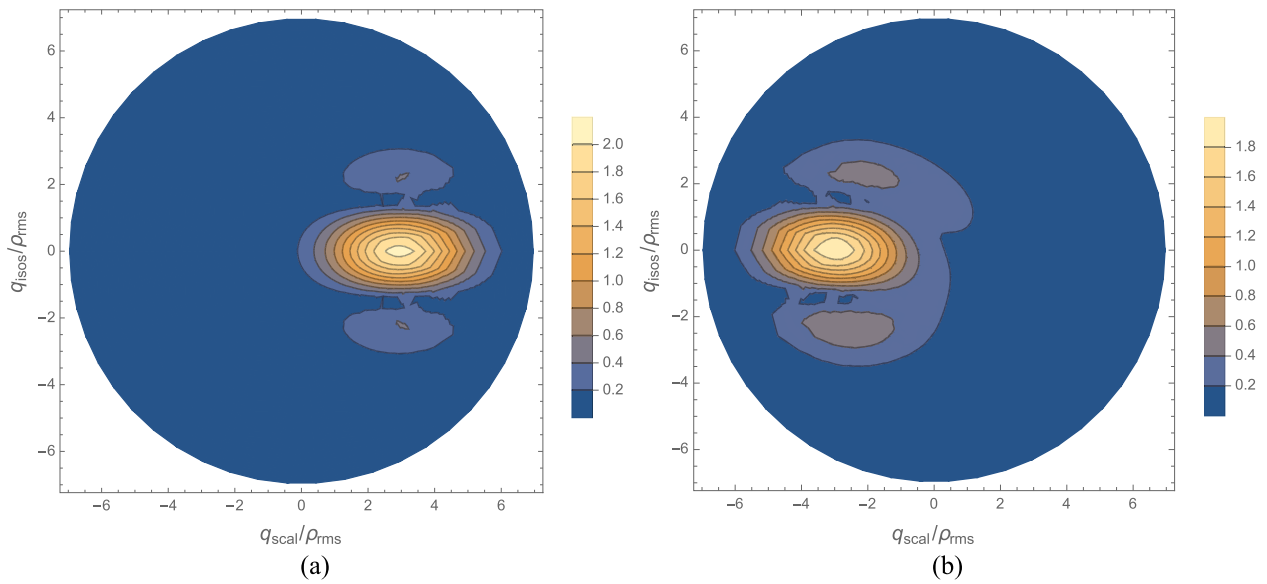

FIG. 10. Propagation of a double wave packet similar to that considered in Fig. 9 but on a single plus-like adiabatic potential surface of unchanging electronic character. In the absence of the nuclear coordinate-dependence of an electronic state participating in a conical intersection, the two components of the double wave packet do not acquire geometric phase factors of opposite sign; after half a period of evolution, constructive rather than destructive interference ensues. The numerical size of the absolute values of the probability amplitude shown here differs from those in Fig. 9 because the symmetric vibrational mode has been suppressed in these calculations. In the present instance, the initial double wave packet is also not "trimmed" by imperfect polarization selection.

Figure 10 plots the evolution of the double wave packet just considered on a two-dimensional potential energy surface identical to $E_+(J_1/\omega_{sym}^2, q_{scal}, q_{isos})$, which, however, is associated with a single, fixed electronic state whose identity does not change with nuclear configuration. In this case, destructive interference does not occur at $\varphi = \pi$ after half a period of clockwise and counterclockwise pseudo-rotation, leading to a nonvanishing probability of observing negative values of the scalene-distortion coordinate.

It is worth noting that, with a limiting choice $\rho_{circ} = -J_1/\omega^2$, equal to the trough radius on the lower Jahn–Teller surface, the classical angular velocity of Eq. (22) would vanish and the two superposed wave packets would become the same. In this situation, analogous to those considered by Izmaylov and co-workers,[53–55] the *spreading* wave packet encircles the conical intersection on both sides, leading to a Berry-phase-induced destructive interference in the probability density. While an initial packet like this one might be easier to generate in some instances, the larger-radius components of the double wave packet considered in Fig. 9 meet up on the opposite side of the conical intersection at well-defined times equal to half-odd multiples of a finite pseudo-rotational period and benefit from the more nearly adiabatic dynamics that occurs at larger ρ_{circ}. Larger pseudo-rotational radii might challenge a harmonic description of the potential or the linear dependence of EET coupling on intermonomer distance, but the geometric nature of the Berry phase would make it resilient to these complications until displacements become so large that they encounter *other* potential-energy crossings.

Observing nodes in the evolving nuclear probability density due to destructive interference would constitute a compelling illustration of the molecular geometric phase effects. (For remarkable recent quantum-simulation experiments that report doing so, see Refs. 64 and 65, discussed in Sec. VI.) Such an observation would not fully characterize molecular Berry phase acquisition, however, since it would fail, for example, to determine which branch of the split wave packet develops which oppositely signed phase factor. The wave-packet interferometry measurements,[46] perhaps, including complete wave-packet reconstruction,[51,52] promise a fuller picture of the molecular geometric phase development. Preparing double wave packets along the lines of Fig. 9 would represent a step toward superposing a target wave packet with an exhaustive family of reference wave packets, as would be required for experimental state reconstruction.

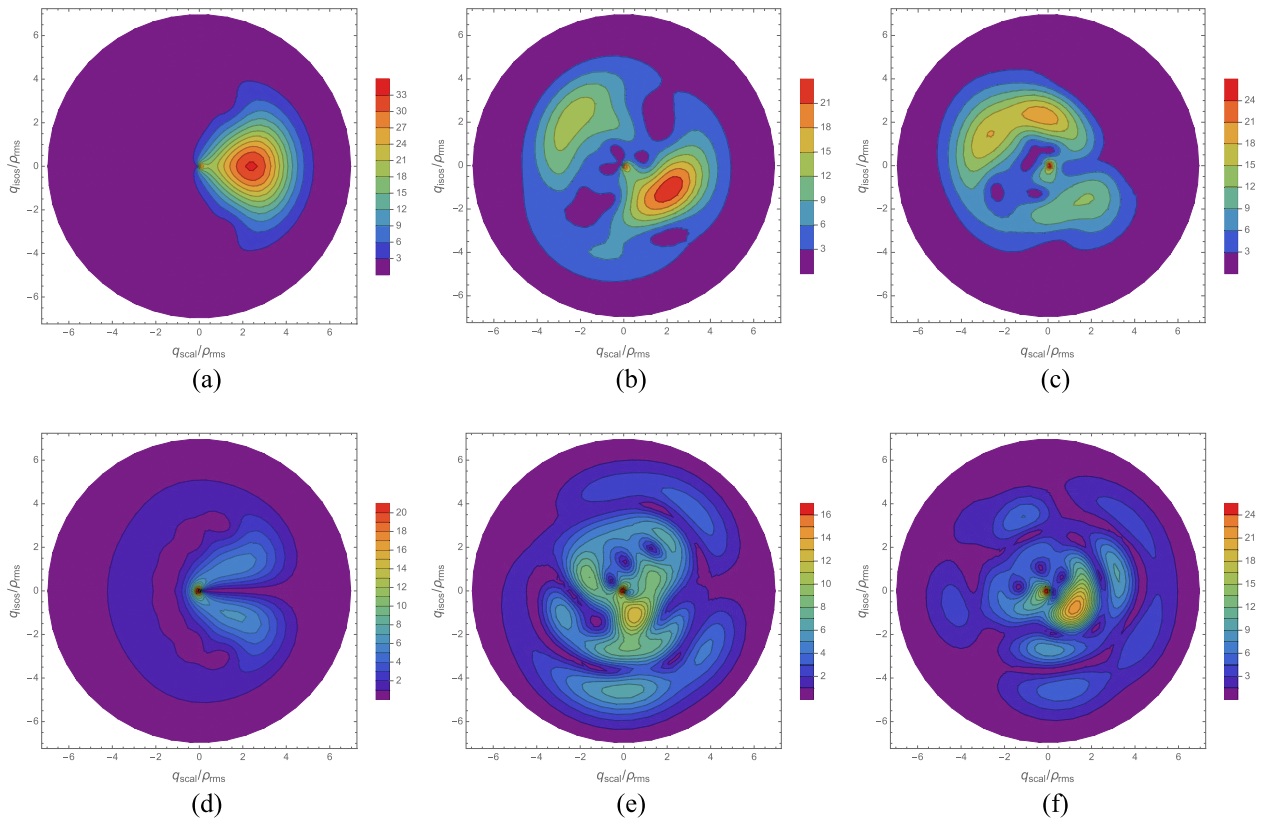

FIG. 11. Contour plots of the absolute value of the evolving distortion-mode nuclear wave packets launched by short-pulse absorption with polarization targeting the minus (upper) Jahn–Teller adiabatic potential-energy surface. The top row shows the evolving wave packet on the upper surface at times 0, τ_-, and $2\tau_-$, from left to right, where τ_- is the period of classical circular pseudo-rotation at the chosen radius on the minus-surface. The bottom row shows the evolving wave packet on the plus (lower) surface, at the same three times, created primarily by the non-adiabatic decay from the upper surface.

V. NON-ADIABATIC DYNAMICS ON THE UPPER JAHN–TELLER SURFACE

While the pseudo-rotational distortion-mode dynamics beginning on the lower Jahn–Teller (plus) surface can remain largely adiabatic in nature, it is to be expected that the motion on the upper (minus) surface will typically be subject to non-adiabatic decay to the lower surface by way of the conical intersection between the two adiabatic potentials.[56] However, Slonczewski and Moruzzi[36] have characterized isolated, high-lying Born–Oppenheimer-like molecular eigenstates on an upper Jahn–Teller surface that are stabilized by pseudo-rotational angular momentum and exhibit long-lived resistance to non-adiabatic decay. It is, therefore, interesting to investigate the dynamical analogs of these Slonczewski resonances by exploring the evolution of pseudo-rotating *wave packets* on the upper surface of our EET trimer and their susceptibility to non-adiabatic transitions.

Figure 11 exhibits the evolving amplitudes on the minus- and plus-surfaces resulting from the short-pulse excitation of a wave packet $|\psi_G(0)\rangle$ in the electronic ground-state having $\langle q_{sym}\rangle = J_1/\omega_{sym}^2$, $\langle q_{scal}\rangle = \rho_{circ} = -2J_1/\omega^2$, and $\langle p_{isos}\rangle = \rho_{circ}\,\dot{\varphi}_- = \sqrt{\rho_{circ}(\omega^2\rho_{circ} - J_1)}$. The polarization of the exciting pulse is determined from $\boldsymbol{\mu}_0 \equiv \langle -(J_1/\omega_{sym}^2, \rho_{circ}, 0)|\hat{\mu}|G\rangle$ in this instance, so as to optimize transfer to the upper cone. The starting wave packet in the minus-adiabatic state, along with those at $\tau_- = 2\pi/\dot{\varphi}_- = 2\pi\sqrt{\rho_{circ}/(\omega^2\rho_{circ} - J_1)}$ and $2\tau_-$, are plotted in the top row. The bottom row shows the amplitudes on the lower surface at the same three times, including those of the small initial plus-state wave packet and the growing amplitudes after one and two minus-state pseudo-rotational periods. While significant non-adiabatic decay is seen to occur, the majority of the amplitude survives on the upper cone after circumnavigating the conical intersection twice. The stabilization of the upper-surface amplitude would be expected to become increasingly effective at larger pseudo-rotational radii.

The latter trend might not be as strong if, at each stage of increasing initial radius, the corresponding pseudo-rotational momentum were directed *radially outward*, rather than perpendicular to the displacement. Figure 12 examines the linear distortion-mode motion of this kind, analogous to that of Fig. 11 and possessing the same vibrational energy but with $\langle p_{scal}\rangle$ rather than $\langle p_{isos}\rangle$ equal to $\sqrt{\rho_{circ}(\omega^2\rho_{circ} - J_1)}$. This arrangement allows the wave packet to flee the intersection-point in its early motion, at the cost of passing through it repeatedly later on. Initially, $\langle p_{scal}\rangle \cong 1.22\omega\langle q_{scal}\rangle$ in this case and the wave packets encounter the conical intersection

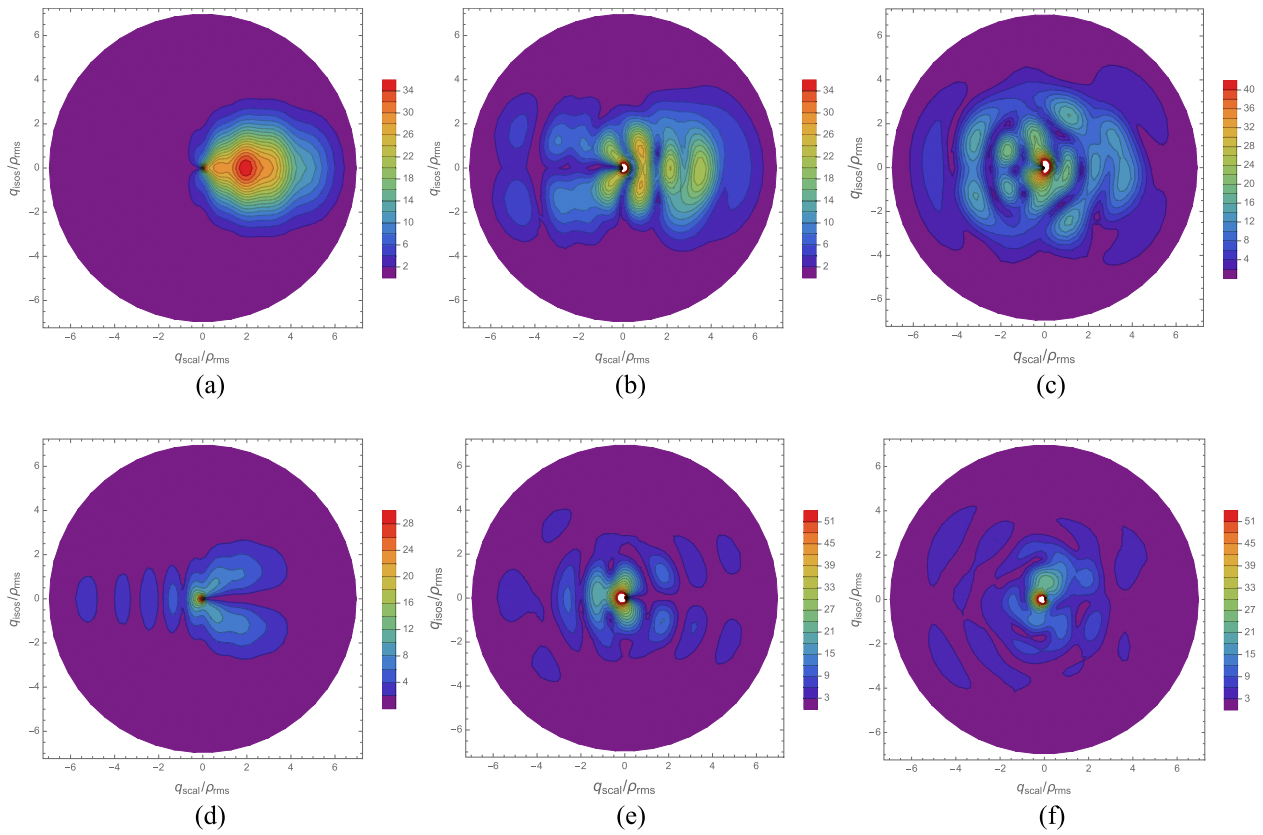

FIG. 12. Same as Fig. 11 but for a distortion-mode wave packet launched on the upper Jahn–Teller adiabatic surface with the initial vibrational momentum directed radially outward. For the sake of comparison, the time intervals are again multiples of τ_-.

repeatedly over the $2\tau_- \cong 1.63\ (2\pi/\omega)$ time-range. The destructive interference resulting from oppositely signed Berry phases is responsible for the node observed on the negative-q_{scal} side of the probability density on the minus-adiabatic surface, which is especially evident in the plot at time τ_- shown in the middle of the upper row in Fig. 12. The adiabatic vector potential responsible for the geometric-phase development may also play a role in the interference processes that occur after or in advance of the non-adiabatic dynamics illustrated by the lower row of this figure.[53] It is interesting to observe that the plus-state wave packet shown in the middle of the lower row in this figure lacks a node on the minus-q_{scal} axis. This behavior is attributable to the fact that $|-(q)\rangle$ for positive q_{scal} and $|+(q)\rangle$ for negative q_{scal} are very similar electronic states, so the wave packet remains focused as it would on a single surface associated with an electronic state of unvarying character.

In this comparison between pseudo-rotational and linear distortion-mode motions, there is not as dramatic a difference between the two cases as would be expected with initial distortions more in excess of the wave-packet width. In both instances, the amplitude non-adiabatically transferred to the lower surface is seen to be concentrated in the Jahn–Teller trough.

VI. CONCLUDING DISCUSSION

The studies of quantum mechanical interference in excitation transfer reported here, along with predictions for the influence of coherent dynamical motion on both electronically adiabatic and non-adiabatic processes in a model EET trimer, provide impetus for further theoretical study and the pursuit of experimental implementation. Numerous data-rich investigations of electronic energy transfer in biophysical and materials-oriented multi-chromophore complexes using phase-coherent ultrafast multi-dimensional spectroscopy testify to a widespread interest in these important fundamental processes and the technical capability to explore them.

An important next step will be to complement the purely dynamical results reported here with simulations that explicitly incorporate initial-state preparation using nonzero-duration laser pulses and the calculation of predicted wave-packet interferometry and other ultrafast-spectroscopy signals. Apart from the processes of the kind considered in Sec. III, which would start with a short-pulse Franck–Condon excitation from a quiescent nuclear configuration, the preparation stage would require externally initiating coherent pseudo-rotational distortion-mode motion in the system's electronic ground-state. This kind of nonstationary change in shape can be driven by impulsive stimulated Raman excitation with crafted sequences of electronically pre-resonant laser pulses,[57] a method that has been demonstrated experimentally[58] and explored further in dynamical simulations[59,60] but whose ultimate capabilities have not yet been tested.

The present study focuses on a threefold symmetric trimer whose monomer transition dipoles are mutually perpendicular. It would be sufficient, though, for those moments to span three-dimensional space. The selective excitation of a given monomer could be driven by a resonant laser pulse that is perpendicular to the transition moments of the other two monomers.

It will be worthwhile to consider the possibility that, in small energy-transfer systems with monomers of different masses and site-energies, certain useful types of coherent structural motion could be initiated by the direct Franck–Condon excitation or using terahertz pulses that address infrared-active modes. In addition, some of the processes considered here are likely to have interesting analogs in trimers of different shapes, including linear configurations.

A current preprint by Makri,[61] investigating electronic frustration and Berry's phase interference in tight-binding models, builds on a prior study by Dani and Makri[62] of excitation transfer in trimeric dendrimers and bears interesting connections to the present work. It considers a cyclic tight-binding trimer with constant coupling parameters and incorporates the interaction of each site with an independent harmonic bath. In one parallel among several, that work examines the effects of interference on population transfer from one site to the other two, a process that may be viewed as the reverse of those considered in Sec. III.

A theoretical study, by Schwennicke and Yuen-Zhou,[63] of induced gauge fields in a molecular homo*tetramer* made use of the Floquet theory to investigate the effect of an elliptically polarized infrared driving field whose frequency is slightly offset from that of a Franck–Condon active intramonomer vibration. It was found that the IR field imposes an excitonic Aharonov–Bohm phase-shift that renders the tetramer optically active to an extent determined solely by that field's ellipticity.

Two recent studies report on the experimental quantum simulations of geometric-phase interference effects[64,65] along the lines considered by Izmaylov and co-workers[53–55] and in Sec. IV B, using trapped atomic ions. Both of these studies employed hyperfine levels of $^{171}Yb^+$ as a qubit representing two molecular electronic levels that participate in a conical intersection and modeled a pair of degeneracy-breaking vibrational modes using the transverse spatial modes of the trapped species. The experiments of Whitlow *et al.*[64] involved five trapped ions, one of whose hyperfine states served as the qubit. The adiabatic state preparation followed by the measurement of the motional-state probability density revealed a node resulting from the destructive interference between the portions of the motional state that bypass the conical intersection on opposite sides. In the experimental simulations of Valahu *et al.*,[65] a single atomic ion provided the qubit and the initial wave packet corresponded to a two-dimensional harmonic oscillator ground state displaced to the circular trough on the lower adiabatic potential of a Jahn–Teller surface. Under its subsequent, nearly adiabatic dynamical evolution, a node of vanishing probability density arose as a result of opposite-sign Berry phase acquisition between the arms of the wave packet that had spread in clockwise and counterclockwise directions about the point of degeneracy.

The model Hamiltonian investigated in this report is designed to illustrate the key processes in the simplest way possible. Further elaboration will be needed in order to make quantitative simulations of dynamics and signals. It is possible that in some EET complexes, a few modes of structural deformation, including changes in intermonomer distances and orientations, will be followed by the vibrationally adiabatic displacement of other, higher-frequency modes, simplifying their theoretical treatment. However, it will be necessary in any case to incorporate additional intramonomer, intermonomer, and host-medium vibrations. Among other features, the effects of nonzero temperature will be important to consider. We

can speculate optimistically that the dynamics seen in Figs. 3, 4, 7–9, 11, and 12, including interference effects, will likely prove resilient to thermal activation of the low-frequency framework-distortion modes, as their behavior would be replicated similarly for each member of a low-temperature ensemble. The thermal effects in a small-multimer excitation transfer have been considered previously by Dani and Makri.[62,61]

ACKNOWLEDGMENTS

The author is grateful for the helpful contributions of Dr. Alexis Kiessling, who participated in discussions on multi-path interference in excitation transfer and in preliminary analyses of the structure and properties of small multimers, and Mr. Eoghan Gormley, who carried out calculations similar to those presented in Figs. 3 and 4. The author would like to thank Professor David Allcock, UO Physics, for telling him about the work in Refs. 25–28, and Alexander Batelaan for a thought-provoking conversation. In addition, the author thanks Victor Romero-Rochín for helpful conversations and Nancy Makri for sharing a relevant preprint. This work was supported by the Grant No. CHE 2102013 from the U.S. National Science Foundation. The author is a member of the labor union United Academics of the University of Oregon, AAUP/AFT Local 3209, AFL-CIO.

AUTHOR DECLARATIONS

Conflict of Interest

The author has no conflicts to disclose.

Author Contributions

Jeffrey A. Cina: Conceptualization (equal); Formal analysis (equal); Funding acquisition (equal); Investigation (equal); Methodology (equal); Project administration (equal); Resources (equal); Writing – original draft (equal); Writing – review & editing (equal).

DATA AVAILABILITY

The data that support the findings of this study are available within the article.

REFERENCES

[1] T. Förster, "Transfer mechanisms of electronic excitation," Discuss. Faraday Soc. **27**, 7–17 (1959).
[2] T. Förster, in *Modern Quantum Chemistry*, edited by O. Sinanoglu (Academic Press, New York, 1965), Vol. 111, p. 93.
[3] S. Rackovsky and R. Silbey, "Electronic energy transfer in impure solids. I. Two molecules embedded in a lattice," Mol. Phys. **25**, 61–72 (1973).
[4] A. Matro and J. A. Cina, "Theoretical studies of time-resolved fluorescence anisotropy from coupled chromophore pairs," J. Phys. Chem. **99**, 2568–2582 (1995).
[5] J. A. Cina, D. S. Kilin, and T. S. Humble, "Wave packet interferometry for short-time electronic energy transfer: Multidimensional optical spectroscopy in the time domain," J. Chem. Phys. **118**, 46–61 (2003).
[6] J. A. Cina and G. R. Fleming, "Vibrational coherence transfer and trapping as sources for long-lived quantum beats in polarized emission from energy transfer complexes," J. Phys. Chem. A **108**, 11196–11208 (2004).
[7] J. D. Biggs and J. A. Cina, "Studies of impulsive vibrational influence on ultrafast electronic excitation transfer," J. Phys. Chem. A **116**, 1683–1693 (2012).
[8] L. Yang, S. Caprasecca, B. Mennucci, and S. Jang, "Theoretical investigation of the mechanism and dynamics of intramolecular coherent resonance energy transfer in soft molecules: A case study of dithia-anthracenophane," J. Am. Chem. Soc. **132**, 16911–16921 (2010).
[9] S. J. Jang, "Effects of donor-acceptor quantum coherence and non-Markovian bath on the distance dependence of resonance energy transfer," J. Phys. Chem. C **123**, 5767–5775 (2019).
[10] C. W. Kim and I. Franco, "Theory of dissipation pathways in open quantum systems," J. Chem. Phys. **154**, 084109 (2021).
[11] M. K. Lee, P. Huo, and D. F. Coker, "Semiclassical path integral dynamics: Photosynthetic energy transfer with realistic environment interactions," Annu. Rev. Phys. Chem. **67**, 639–668 (2016).
[12] S. A. Oh, D. F. Coker, and D. A. W. Hutchinson, "Optimization of energy transport in the Fenna-Matthews-Olson complex via site-varying pigment-protein interactions," J. Chem. Phys. **150**, 085102 (2019).
[13] T. Renger, "Semiclassical modified Redfield and generalized Förster theories of exciton relaxation/transfer in light harvesting complexes: The quest for the principle of detailed balance," J. Phys. Chem. B **125**, 6406–6416 (2021).
[14] S. Kundu, R. Dani, and N. Makri, "B800-to-B850 relaxation of excitation energy in bacterial light harvesting: All-state, all-mode path integral simulations," J. Chem. Phys. **157**, 015101 (2022).
[15] J. Kim, T. C. Nguyen-Phan, A. T. Gardiner, R. J. Cogdell, G. D. Scholes, and M. Cho, "Low-frequency vibronic mixing modulates the excitation energy flow in bacterial light-harvesting complex II," J. Phys. Chem. Lett. **12**, 6292–6298 (2021).
[16] J. Kim, T. C. Nguyen-Phan, A. T. Gardiner, T. H. Yoon, R. J. Cogdell, M. Cho, and G. D. Scholes, "Vibrational modes promoting exciton relaxation in the B850 band of LH2," J. Phys. Chem. Lett. **13**, 1099–1106 (2022).
[17] D. Heussman, J. Kittell, P. H. von Hippel, and A. H. Marcus, "Temperature-dependent local conformations and conformational distributions of cyanine dimer labeled single-stranded–double-stranded DNA junctions by 2D fluorescence spectroscopy," J. Chem. Phys. **156**, 045101 (2022).
[18] M. Cho, *Two-Dimensional Optical Spectroscopy* (CRC Press, Boca Raton, 2009).
[19] S. Mukamel, "Multidimensional femtosecond correlation spectroscopies of electronic and vibrational excitations," Annu. Rev. Phys. Chem. **51**, 691–729 (2000).
[20] D. M. Jonas, "Two-dimensional femtosecond spectroscopy," Annu. Rev. Phys. Chem. **54**, 425–463 (2003).
[21] E. Harel, "Four-dimensional coherent electronic Raman spectroscopy," J. Chem. Phys. **146**, 154201 (2017).
[22] J. A. Cina, *Getting Started on Time-Resolved Molecular Spectroscopy* (Oxford University Press, New York, 2022).
[23] G. D. Scholes, G. R. Fleming, L. X. Chen, A. Aspuru-Guzik, A. Buchleitner, D. F. Coker, G. S. Engel, R. van Grondelle, A. Ishizaki, D. M. Jonas, J. S. Lundeen, J. K. McCusker, S. Mukamel, J. P. Ogilvie, A. Olaya-Castro, M. A. Ratner, F. C. Spano, K. B. Whaley, and X. Zhu, "Using coherence to enhance function in chemical and biophysical systems," Nature **543**, 647–656 (2017).
[24] J. Cao, R. J. Cogdell, D. F. Coker, H.-G. Duan, J. Hauer, U. Kleinekathöfer, T. L. C. Jansen, T. Mančal, R. J. D. Miller, J. P. Ogilvie, V. I. Prokhorenko, T. Renger, H.-S. Tan, R. Tempelaar, M. Thorwart, E. Thyrhaug, S. Westenhoff, and D. Zigmantas, "Quantum biology revisited," Sci. Adv. **6**, eaaz4888 (2020).
[25] A. Noguchi, Y. Shikano, K. Toyoda, and S. Urabe, "Aharonov-Bohm effect in the tunnelling of a quantum rotor in a linear Paul trap," Nat. Commun. **5**, 3868 (2014).
[26] D. J. Gorman, B. Hemmerling, E. Megidish, S. A. Moeller, P. Schindler, M. Sarovar, and H. Haeffner, "Engineering vibrationally assisted energy transfer in a trapped-ion quantum simulator," Phys. Rev. X **8**, 011038 (2018).
[27] F. Hakelberg, P. Kiefer, M. Wittemer, U. Warring, and T. Schaetz, "Interference in a prototype of a two-dimensional ion trap array quantum simulator," Phys. Rev. Lett. **123**, 100504 (2019).

[28]U. Warring, F. Hakelberg, P. Kiefer, M. Wittemer, and T. Schaetz, "Trapped ion architecture for multi-dimensional quantum simulations," Adv. Quantum Technol. **3**, 1900137 (2020).
[29]H. C. Longuet-Higgins, "Some recent developments in the theory of molecular energy levels," Adv. Spectrosc. **2**, 429–472 (1961).
[30]C. A. Mead and D. G. Truhlar, "On the determination of Born–Oppenheimer nuclear motion wave functions including complications due to conical intersections and identical nuclei," J. Chem. Phys. **70**, 2284–2296 (1979).
[31]M. V. Berry and M. Wilkinson, "Diabolical points in the spectra of triangles," Proc. R. Soc. London, Ser. A **392**, 15–43 (1984).
[32]M. V. Berry, "Quantal phase factors accompanying adiabatic changes," Proc. R. Soc. London, Ser. A **392**, 45–57 (1984).
[33]*Geometric Phases in Physics*, edited by F. Wilczek and A. Shapere (World Scientific, Singapore, 1989).
[34]C. A. Mead, "The geometric phase in molecular systems," Rev. Mod. Phys. **64**, 51–85 (1992).
[35]D. R. Yarkony, "Perspective on 'Some recent developments in the theory of molecular energy levels,'" Theor. Chem. Acc. **103**, 242–247 (2000).
[36]J. C. Slonczewski and V. L. Moruzzi, "Excited states in the dynamic Jahn–Teller effect," Physics **3**, 237–254 (1967).
[37]R. Dani and N. Makri, "Time-evolving quantum superpositions in open systems and the rich content of coherence maps," J. Phys. Chem. B **126**, 9361–9375 (2022).
[38]A. J. Kiessling and J. A. Cina, "Monitoring the evolution of intersite and interexciton coherence in electronic excitation transfer via wave-packet interferometry," J. Chem. Phys. **152**, 244311 (2020).
[39]S. Tomasi and I. Kassal, "Classification of coherent enhancements of light-harvesting processes," J. Phys. Chem. Lett. **11**, 2348–2355 (2020).
[40]J. Cao and R. J. Silbey, "Optimization of exciton trapping in energy transfer processes," J. Phys. Chem. A **113**, 13825–13838 (2009).
[41]S. Jang, "Theory of multichromophoric coherent resonance energy transfer: A polaronic quantum master equation approach," J. Chem. Phys. **135**, 034105 (2011).
[42]G. Engelhardt and J. Cao, "Tuning the Aharonov-Bohm effect with dephasing in nonequilibrium transport," Phys. Rev. B **99**, 075436 (2019).
[43]H. Hossein-Nejad, A. Olaya-Castro, and G. D. Scholes, "Phonon-mediated path-interference in electronic energy transfer," J. Chem. Phys. **136**, 024112 (2012).
[44]S. S. Skourtis, D. H. Waldeck, and D. N. Beratan, "Inelastic electron tunneling erases coupling-pathway interferences," J. Phys. Chem. B **108**, 15511–15518 (2004).
[45]D. N. Beratan, S. S. Skourtis, I. A. Balabin, A. Balaeff, S. Keinan, R. Venkatramani, and D. Xiao, "Steering electrons on moving pathways," Acc. Chem. Res. **42**, 1669–1678 (2009).
[46]J. A. Cina, T. J. Smith, Jr., and V. Romero-Rochin, "Time-resolved optical tests for electronic geometric phase development," Adv. Chem. Phys. **83**, 1–42 (1993).
[47]J. A. Cina, "Phase-controlled optical pulses and the adiabatic electronic sign change," Phys. Rev. Lett. **66**, 1146–1149 (1991).
[48]V. Romero-Rochin and J. A. Cina, "Time development of geometric phases in the Longuet-Higgins model," J. Chem. Phys. **91**, 6103–6112 (1989).
[49]S. K. Min, A. Abedi, K. S. Kim, and E. K. U. Gross, "Is the molecular Berry phase an artifact of the Born–Oppenheimer approximation?," Phys. Rev. Lett. **113**, 263004 (2014).
[50]Y.-C. Shen and J. A. Cina, "What can short-pulse pump-probe spectroscopy tell us about Franck-Condon dynamics?," J. Chem. Phys. **110**, 9793–9806 (1999).
[51]T. S. Humble and J. A. Cina, "Nonlinear wave-packet interferometry and molecular state reconstruction in a vibrating and rotating diatomic molecule," J. Phys. Chem. B **110**, 18879–18892 (2006).
[52]J. A. Cina, "Wave-packet interferometry and molecular state reconstruction: Spectroscopic adventures on the left-hand side of the Schrödinger equation," Annu. Rev. Phys. Chem. **59**, 319–342 (2008).
[53]I. G. Ryabinkin, L. Joubert-Doriol, and A. F. Izmaylov, "Geometric phase effects in nonadiabatic dynamics near conical intersections," Acc. Chem. Res. **50**, 1785–1793 (2017).
[54]S. Henshaw and A. F. Izmaylov, "Topological origins of bound states in the continuum for systems with conical intersections," J. Phys. Chem. Lett. **9**, 146–149 (2018).
[55]L. Joubert-Doriol and A. F. Izmaylov, "Molecular 'topological insulators': A case study of electron transfer in the bis(methylene) adamantyl carbocation," Chem. Commun. **53**, 7365 (2017).
[56]*Conical Intersections: Theory, Computation and Experiment*, edited by W. Domcke, D. R. Yarkony, and H. Köppel (World Scientific, Singapore, 2011).
[57]J. A. Cina and V. Romero-Rochin, "Optical impulsive excitation of molecular pseudorotation in Jahn–Teller systems," J. Chem. Phys. **93**, 3844–3849 (1990).
[58]M. M. Wefers, H. Kawashima, and K. A. Nelson, "Optical control over two-dimensional lattice vibrational trajectories in crystalline quartz," J. Chem. Phys. **108**, 10248–10255 (1998).
[59]T. J. Smith and J. A. Cina, "Toward preresonant impulsive Raman preparation of large amplitude vibrational motion," J. Chem. Phys. **104**, 1272–1292 (1996).
[60]J. A. Cina, "On impulsive excitation of pseudorotation for geometric phase detection," J. Raman Spectrosc. **31**, 95–97 (2000).
[61]N. Makri, "Electronic frustration, Berry's phase interference and slow dynamics in some tight-binding systems coupled to harmonic baths," J. Phys. A: Math. Theor. **56**, 144001 (2023).
[62]R. Dani and N. Makri, "Excitation energy transfer in bias-free dendrimers: Eigenstate structure, thermodynamics, and quantum evolution," J. Phys. Chem. C **126**, 10309–10319 (2022).
[63]K. Schwennicke and J. Yuen-Zhou, "Optical activity from the exciton Aharonov-Bohm effect: A Floquet engineering approach," J. Phys. Chem. C **124**, 4206–4214 (2020).
[64]J. Whitlow, Z. Jia, Y. Wang, C. Fang, J. Kim, and K. R. Brown, "Simulating conical intersections with trapped ions," arXiv:2211.07319v2 [quant-ph].
[65]C. H. Valahu, V. C. Olaya-Agudelo, R. J. MacDonell, T. Navickas, A. D. Rao, M. J. Millican, J. B. Pérez-Sánchez, J. Yuen-Zhou, M. J. Biercuk, C. Hempel, T. R. Tan, and I. Kassal, "Direct observation of geometric phase in dynamics around a conical intersection," arXiv:2211.07320v2 [quant-ph].